International Journal of Power Electronics and Drive System (IJPEDS)
Vol. 17, No. 1, March 2026, pp. 180~194
ISSN: 2088-8694, DOI: 10.11591/ijpeds.v17.i1.pp180-194

Fuzzy logic direct torque control of induction motors using three-level NPC inverter

Jamila Chennane[1], Lahcen Ouboubker[1], Mohamed Akhsassi[2]
[1]MS3E Laboratory, Faculty of Applied Sciences of Ait Melloul, Ibn Zohr University, Agadir, Morocco
[2]LGEMS Laboratory, National School of Applied Sciences of Agadir, Ibn Zohr University, Agadir, Morocco

Article Info

Article history:

Received Oct 2, 2025
Revised Jan 18, 2026
Accepted Feb 15, 2026

Keywords:

Direct torque control
Fuzzy logic
Induction motor
NPC inverter
Renewable energy
Torque ripple reduction

ABSTRACT

Induction motor drives are extensively used for their robustness and efficiency, but precise control remains difficult under dynamic conditions. Conventional direct torque control offers a simple structure and fast response, but is limited by torque ripple, flux distortion, and poor low-speed performance. This paper proposes a fuzzy logic-based direct torque control (FDTC) combined with a three-level neutral point clamped (NPC) inverter. A fuzzy inference system (FIS) replaces the hysteresis comparators and switching table, while speed regulation is improved using a PI-fuzzy controller. MATLAB/Simulink simulations under speed variations and load disturbances demonstrate reduced torque and flux ripples, smoother flux trajectories, improved current waveforms, and faster transient response compared with classical DTC. These results confirm that the FDTC–NPC approach provides a robust and efficient solution for advanced applications such as industrial automation, renewable energy, and electric vehicles.

Corresponding Author:

Jamila Chennane
MS3E Laboratory, Faculty of Applied Sciences of Ait Melloul, Ibn Zohr University
Agadir, Morocco
Email: jamila.chennane@gmail.com

1. INTRODUCTION

Induction motor (IM) drives are still used in current industrial systems because they are more robust, reliable, and cost-effective than DC machines [1], [2]. They are widely used in automation, renewable energy, and electric car applications where accurate torque and flux control are critical. Nevertheless, the nonlinear dynamics and parameter fluctuations of IMs make their control intrinsically difficult.

Following the advent of power electronics, multilevel inverter topologies, particularly the three-level neutral point clamped (NPC) inverter, have emerged as efficient solutions that provide decreased harmonic distortion, reduced voltage stress, and improved output quality [3]-[5]. Direct torque control (DTC), first developed by Takahashi and Noguchi [4] and later refined by Depenbrock [5], is well-known for its simple structure, quick torque response, and little reliance on machine parameters [6]. However, the standard two-level DTC has significant torque and flux ripples, as well as variable switching frequency, particularly at low speeds [7]. Advanced approaches, such as space vector modulation (SVM) [8] and model predictive control (MPC) [9], address these difficulties while increasing complexity and processing burden.

To address these constraints, intelligent control approaches have been implemented into DTC systems. Fuzzy logic control (FLC) has showed exceptional capacity to handle nonlinearities and parameter fluctuations while maintaining robustness and quick dynamics. The use of fuzzy reasoning allows for continuous voltage-vector selection, smoother electromagnetic transitions, and near-constant switching frequency [10]-[16]. Furthermore, coupling FLC with the enlarged voltage-vector set of the three-level NPC inverter increases flux trajectory smoothness, reduces total harmonic distortion (THD), and improves steady-

state efficiency. Despite these benefits, few research has thoroughly examined fuzzy inference mechanisms in multilevel inverter-fed DTC schemes. In particular, the combined use of fuzzy decision layers and the richer voltage-vector structure of three-level NPC inverters has received insufficient attention for increasing torque ripple suppression and low-speed robustness under dynamic operating conditions.

This work presents an improved fuzzy direct torque control (FDTC) technique for induction motor drives based on a three-level NPC inverter. The fuzzy inference system substitutes traditional hysteresis comparators and lookup tables for voltage-vector selection, and a PI-Fuzzy speed regulator improves adaptability and transient response. The proposed FDTC-NPC technique is tested using MATLAB/Simulink simulations under various load and speed situations, which show reduced torque and flux ripples, enhanced steady-state precision, and superior dynamic behavior when compared to classical DTC.

2. METHODOLOGY OF DTC AND THREE-LEVEL INVERTERS

2.1. Principle of conventional direct torque control

DTC, initially introduced by Takahashi and Noguchi [4] and later refined by Depenbrock [5], is a well-established technique for high-performance IM drives. It directly controls electromagnetic torque and stator flux without requiring coordinate transformations or pulse width modulation, offering a simpler and faster alternative to FOC [8]. As illustrated in Figure 1, the classical DTC structure includes a flux and torque estimator, hysteresis comparators, a sector selector, and a voltage vector switching table. The estimated torque and flux are continuously compared with their reference values, and the resulting control signals determine the inverter's switching states. While DTC provides fast responsiveness and resistance to parameter fluctuations, it suffers from significant torque ripple and variable switching behavior, resulting in poor performance at low rotational speeds. These restrictions encourage the employment of multiple inverters and adaptive control techniques to increase torque smoothness, flux management, and stable state performance.

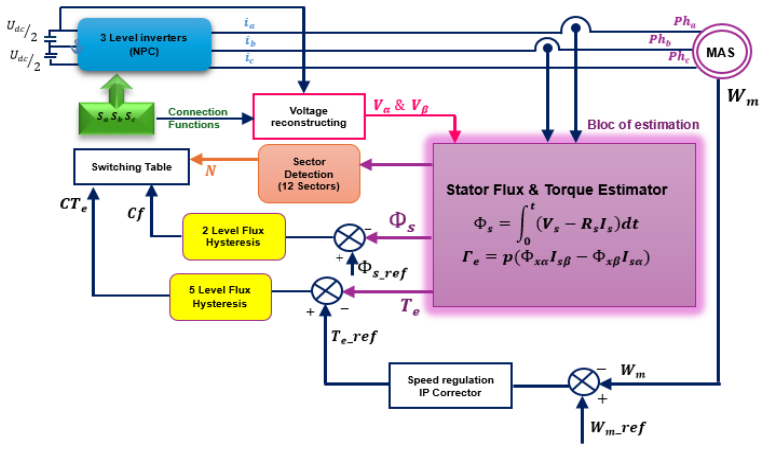

Figure 1. Block diagram of the conventional DTC applied to a three-level inverter-fed IM

2.2. Mathematical modeling

The dynamic behavior of the IM in the stationary (α, β) reference frame can be expressed by the stator voltage equations derived from the classical DTC formulation and vector control theory [2], [5], [7]-[9]. These components are given by (1).

$$V_{s\alpha} = R_s I_{s\alpha} + \frac{d\Phi_{s\alpha}}{dt} \qquad V_{s\beta} = R_s I_{s\beta} + \frac{d\Phi_{s\beta}}{dt} \tag{1}$$

The stator-flux components are obtained by integrating the voltage equations, which form the basis of flux estimation in DTC schemes [2], [5], [8]:

$$\Phi_{s\alpha} = \int_0^t (V_{s\alpha} - R_s I_{s\alpha})\, dt \qquad \Phi_{s\beta} = \int_0^t (V_{s\beta} - R_s I_{s\beta}) dt \tag{2}$$

The stator flux is mathematically defined by (3).

$$\Phi_s = \sqrt{\Phi^2{}_{s\alpha} + \Phi^2{}_{s\beta}} \tag{3}$$

The stator flux angle is determined using (4).

$$\theta_s = tan^{-1}(\Phi_{s\beta} / \Phi_{s\alpha}) \tag{4}$$

These quantities are crucial for real-time sector identification and torque/flux control in DTC and FDTC algorithms [7], [8], [17]. The electromagnetic torque developed by the machine is given by (5).

$$\Gamma_e = p(\Phi_{s\alpha} I_{s\beta} - \Phi_{s\beta} I_{s\alpha}) \tag{5}$$

This approach, developed by Takahashi and Noguchi [4] and revised by Depenbrock [5], provides the mathematical foundation for DTC. The (1)-(4) define the electromagnetic interaction of stator voltage $V_{sa}, V_{s\beta}$, current, and flux vectors. They are numerically implemented in the DTC estimator to estimate the instantaneous electromagnetic torque and stator flux, which are then continually compared to their reference values using hysteresis controllers. The above formulation has undergone extensive validation for both traditional and multilevel inverter-fed DTC systems [8], [9].

2.3. Switching logic and sector selection

In conventional DTC, electromagnetic torque and stator flux from (1)-(4) are compared to references via hysteresis comparators, maintaining values within tolerance bands through real-time switching state adjustments [9], [10]. Two independent controllers for flux and torque generate binary outputs for example flux signal C_f which, combined with stator flux position (α, β), select the applied voltage vector. This enables rapid torque response without coordinate transformations or PWM modulators [11].

$$C_f = \begin{cases} +1 \; if \; \Phi_s < \Phi_{sref} \; (\text{Flux must increase}) \\ -1 \; if \; \Phi_s > \Phi_{sref} \; (\text{Flux must decrease}) \end{cases} \tag{6}$$

As shown in Figure 2, this two-level decision process stabilizes the flux amplitude around its reference value Φ_s^* and prevents excessive oscillations. The torque comparator, on the other hand, evaluates the torque error $\Delta\Gamma_e = \Gamma_e^* - \Gamma_e$ and generates a discrete control signal $C_T \in \{-2, -1, 0, +1, +2\}$, corresponding to large positive, small positive, zero, small negative, and large negative torque variations. This five-level quantization enables finer torque control and smoother electromagnetic transitions than conventional two-level methods [12], [13].

The DTC algorithm assesses both flux and torque error rate, estimates the stator flux sector using (4), and selects a voltage vector from the triplet (C_f, C_T, N) [12], [13]. A two-level inverter uses six 60° sectors in the (α, β) plane, but a three-level NPC uses twelve 30° sectors for better voltage-vector resolution and smoother flux transitions [14]-[16]. This selecting mechanism guarantees quick torque response and reliability under various loads. However, the limited vectors in two-level inverters generate torque ripple and variable switching frequency, which supports the NPC topology's superior steady-state and dynamic performance.

In stator-flux regulation, a two-level hysteresis comparator is employed to ensure the flux magnitude remains within a specified tolerance band of $\mp\Delta\Phi_s$. As shown in Figure 3, the comparator produces the discrete control signal $C_f \in [-1, 1]$, which signifies if the calculated stator flux exceeds its reference beyond the permissible hysteresis boundaries [9], [10].

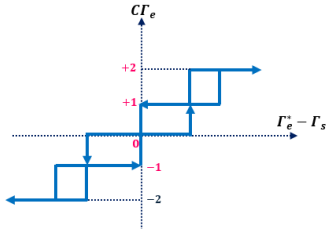

Figure 2. Five-level hysteresis comparator used for electromagnetic torque regulation

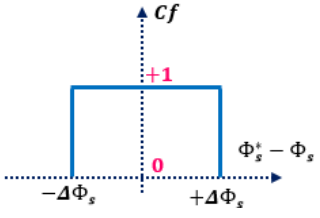

Figure 3. Two-level hysteresis comparator for stator-flux regulation

When the estimated flux exceeds the upper limit of the band, a negative control action is implemented to diminish the flux magnitude; conversely, when it drops below the lower limit, a positive control action is enacted to restore it. This hysteresis-based technique guarantees that the stator-flux amplitude remains constrained around its reference value while maintaining the rapid dynamic response and structural simplicity inherent in traditional DTC schemes.

2.4. Extension to the three-level NPC inverter

In this topology, as illustrated in Figure 4, the total DC-link voltage E is symmetrically divided across two series-connected capacitors, producing three distinct output voltage levels per phase: $(+E/2, 0, -E/2)$ [18], [19]. This arrangement reduces voltage stress on switching devices and improves the output waveform quality compared to conventional two-level inverters

The switching states of the devices determine the instantaneous phase voltage V_i applied to the motor stator winding. The corresponding binary switching functions for the upper and lower branches can be expressed as (7).

$$S_{i1}^b = S_{i1} x\, S_{i2},\ S_{i0}^b = S_{i3} x\, S_{i4} \quad with\ the\ S_i \in \{+1, 0-1\}, \tag{7}$$

The corresponding phase-to-neutral voltage of phase $i \in \{a, b, c\}$ is expressed as (8).

$$V_{iO} = \frac{E}{2} S_i = \frac{E}{2}(S_{i1}^b - S_{i0}^b) \tag{8}$$

Where $S_{i1}^b = 1$ corresponds to $+E/2$, $S_{i0}^b = 1$ corresponds to $-E/2$ and both equal to 0 represents the zero state connected to the midpoint through the clamping diodes. The output phase voltages (V_a, V_b, V_c) relative to the neutral point O are expressed as (9).

$$\begin{bmatrix} V_a \\ V_b \\ V_c \end{bmatrix} = \frac{E}{v} \begin{bmatrix} 2 & -1 & -1 \\ -1 & 2 & -1 \\ -1 & -1 & 2 \end{bmatrix} x \left\{ \begin{bmatrix} S_{11}^b \\ S_{21}^b \\ S_{31}^b \end{bmatrix} - \begin{bmatrix} S_{10}^b \\ S_{20}^b \\ S_{30}^b \end{bmatrix} \right\} \tag{9}$$

The switching combinations yield 27 states, 19 of which correspond to different voltage vectors in the (α, β) plane [20]. Vectors are divided into three types based on their magnitude: large, medium, and small. Large vectors allow for quick torque and flux fluctuations, while medium vectors provide smoother transient transitions. Small vectors ensure precision flux control and little torque ripple.

Figure 5 illustrates their spatial organization, with big vectors forming the outer hexagon, medium vectors in intermediate places, and small vectors concentrated around the plane's core. Figure 6 shows how the (α, β) plane is divided into twelve equal 30° sectors to allow for real-time stator-flux position and vector selection. This subdivision enhances torque and flux management by reducing vector steps and resulting in more uniform flux trajectories [21], [22].

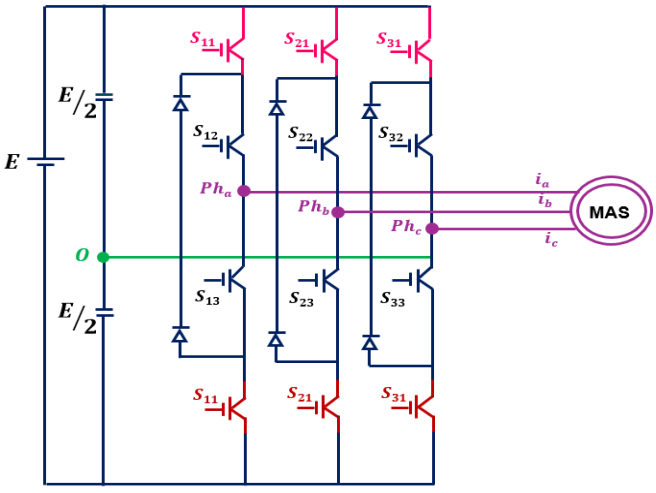

Figure 4. Structure of the three-level NPC inverter

The primary switching combinations for each phase leg are summarized in Table 1, where "ON" and "OFF" denote conducting and non-conducting states of the power devices, respectively. This topology keeps the DC-link voltage balanced and allows for symmetrical operation. This reduces switching stress and harmonic distortion. The extra voltage level improves current quality and lowers acoustic noise compared to the two-level inverter [23]. When used in DTC, the NPC inverter allows for smoother transitions in torque and flux, a nearly constant switching frequency, and better low-speed stability. This makes it a suitable platform for better control strategies like FDTC.

2.5. Control rule table for DTC with three-level NPC inverter

In three-level NPC-based DTC, voltage vector selection uses the triplet (C_f, C_T, N) to represent flux error, torque error, and stator-flux sector. This helps choose from 27 switching states (19 unique vectors) [20], [21]. The expanded vector set allows for better control. Large vectors handle quick torque changes, while small and medium vectors reduce switching stress and current distortion. This results in smoother flux paths and a more stable switching frequency [22]-[24]. Table 2 summarizes the sector-based logic. It links each 30° sector to the control action needed for accurate torque regulation and stable drive performance [25], [26].

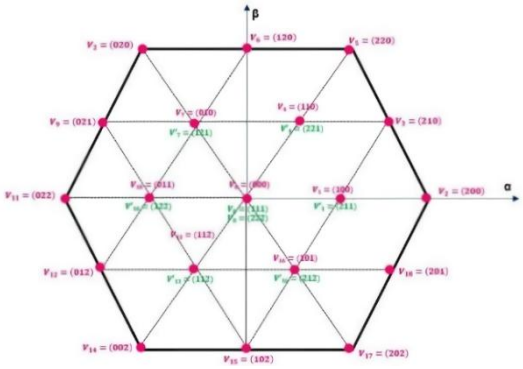

Figure 5. Space-vector representation of the 27 switching states of the NPC inverter

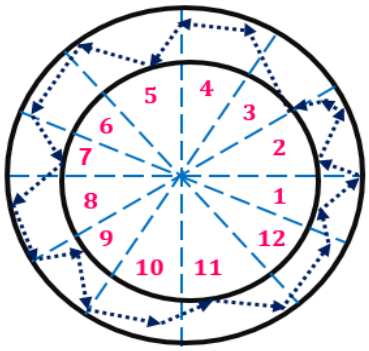

Figure 6. Sector division of the (α, β) flux plane for three-level NPC inverter switching

Table 1. Switching combinations and corresponding output levels for a single NPC inverter leg

Switching state	S_{i1}	S_{i1}	S_{i2}	S_{i3}	S_{i4}	Output voltage V_i
+1	ON	ON	ON	OFF	OFF	$E/2$
0	OFF	OFF	ON	ON	OFF	0
-1	OFF	OFF	OFF	ON	ON	$-E/2$

Table 2. Switching table for DTC with a three-level NPC inverter

N_1			N_2			N_7			N_8		
C_{Te}/C_r	1	0	C_{Te}/C_r	1	0	C_{Te}/C_r	1	0	C_{Te}/C_r	1	0
+2	V_5	V_8	+2	V_5	V_8	+2	V_{14}	V_{17}	+2	V_{14}	V_{17}
+1	V_4	V_7	+1	V_4	V_7	+1	V_{13}	V_{16}	+1	V_{13}	V_{16}
0	V_{19}	V_{20}	0	V_{20}	V_{19}	0	V_{19}	V_{20}	0	V_{20}	V_{19}
-1	V_{16}	V_{13}	-1	V_{16}	V_{13}	-1	V_7	V_4	-1	V_7	V_4
-2	V_{17}	V_{14}	-2	V_2	V_{17}	-2	V_8	V_5	-2	V_{11}	V_5
N_3			N_4			N_9			N_{10}		
C_{Te}/C_r	1	0	C_{Te}/C_r	1	0	C_{Te}/C_r	1	0	C_{Te}/C_r	1	0
+2	V_8	V_{11}	+2	V_8	V_{11}	+2	V_{17}	V_2	+2	V_{17}	V_2
+1	V_7	V_{10}	+1	V_7	V_{10}	+1	V_{16}	V_1	+1	V_{16}	V_1
0	V_{19}	V_{20}	0	V_{20}	V_{19}	0	V_{19}	V_{20}	0	V_{20}	V_{19}
-1	V_1	V_{16}	-1	V_1	V_{16}	-1	V_{10}	V_7	-1	V_{10}	V_7
-2	V_2	V_{17}	-2	V_5	V_2	-2	V_{11}	V_8	-2	V_{14}	V_{11}
N_5			N_6			N_{11}			N_{12}		
C_{Te}/C_r	1	0	C_{Te}/C_r	1	0	C_{Te}/C_r	1	0	C_{Te}/C_r	1	0
+2	V_{11}	V_{14}	+2	V_{11}	V_{14}	+2	V_2	V_5	+2	V_2	V_5
+1	V_{10}	V_{13}	+1	V_{10}	V_{13}	+1	V_1	V_4	+1	V_1	V_4
0	V_{19}	V_{20}	0	V_{20}	V_{19}	0	V_{19}	V_{20}	0	V_{20}	V_{19}
-1	V_4	V_1	-1	V_4	V_1	-1	V_{13}	V_{10}	1	V_{13}	V_{10}
-2	V_5	V_2	-2	V_8	V_5	-2	V_{14}	V_{11}	-2	V_{17}	V_{14}

2.6. IP speed controller synthesis

The IP speed controller is widely used in high-performance IM drives for its fast dynamics and its ability to eliminate zeros in the closed-loop transfer function, ensuring a continuous torque reference during transients [27], [28]. As shown in Figure 7, the speed error $\Omega^*(s) - \Omega(s)$ is processed through proportional and integral paths scaled by $K_{\Omega p}$, $K_{\Omega i}$ respectively, to generate the reference torque $\Gamma_r(s)$ which governs the machine's electromagnetic response [29]. The mechanical dynamics of the IM can be modeled as:

$$F(s) = \frac{1}{Js+f} \tag{10}$$

assuming no external load disturbances $T_r = 0$, the closed-loop transfer function between reference speed $\Omega^*(s)$ and actual speed $\Omega(s)$ is given by [30]:

$$\frac{\Omega(s)}{\Omega^*(s)} = \frac{1}{\frac{\tau_1}{g_1 K_{\Omega i}} s^2 + \frac{1}{g_1 K_{\Omega i}} s + 1} \tag{11}$$

where the parameters τ_1 and g_1 are defined by:

$$\tau_1 = \frac{J}{K_{\Omega p}+f} \tag{12}$$

$$g_1 = \frac{K_{\Omega p}}{K_{\Omega p}+f} \tag{13}$$

here, $K_{\Omega p}$ and $K_{\Omega i}$ denote the proportional and integral gains of the IP controller, respectively. To achieve an aperiodic speed response, the controller gains must satisfy:

$$K_{\Omega i} = \frac{1}{4 g_1 \tau_1} \tag{14}$$

and under these conditions, the equivalent time constant of the closed-loop dynamics becomes:

$$\tau_2 = 2\tau_1 \tag{15}$$

consequently, the proportional gain is obtained as (16).

$$K_{\Omega p} = \frac{J - \tau_1 f}{\tau_1} \tag{16}$$

This systematic tuning method ensures smooth torque response, strong disturbance rejection, and stable operation across a wide range of speeds. The IP controller thus provides an effective balance between simplicity, robustness, and dynamic accuracy in DTC–NPC-based drives [27], [30].

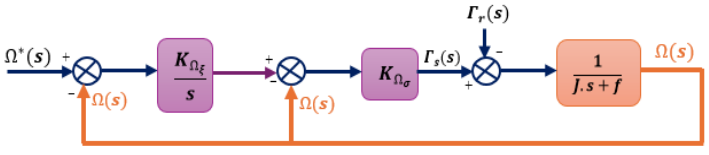

Figure 7. Closed-loop speed regulation using an IP controller

3. FUZZY DIRECT TORQUE CONTROL

3.1. Principle of FDTC

A combination of hysteresis comparators and fixed switching tables, conventional DTC has poor low-speed efficiency, variable switching frequency, and torque ripple. By substituting an FIS for them, the FDTC approach solves these problems and permits adaptive and continuous voltage-vector selection [31]-[33]. To find the ideal inverter vector that minimizes flux and torque deviations while maintaining neutral-point balance, the fuzzy block in the proposed FDTC–NPC scheme, as illustrated in Figure 8, processes the stator flux error Δ^1, torque error $\Delta\Gamma$, and stator flux angle $\theta \in [-\pi, \pi]$.

The input variables of the fuzzy system are defined as (17).

$$\Delta\Phi_s = \Phi_s^* - \Phi_s \qquad \Delta\Gamma_e = \Gamma_e^* - \Gamma_e \tag{17}$$

Where Φ_s^* and Γ_e^* are the reference stator flux and torque, respectively. The control objective is to minimize both errors within the permissible tolerance band: $min\{|\Delta\Phi_s|, |\Delta\Gamma_e|\}$. The fuzzy inference mechanism processes these inputs through a rule base that relates flux and torque errors to a corresponding output voltage vector $V_{\alpha\beta}$:

$$V_{\alpha\beta} = f(\Delta\Phi_s, \Delta\Gamma_e, \theta_s) \tag{18}$$

The fuzzy mapping function $f(.)$ directly synthesizes the optimal voltage vector from expert rules and the sector index. This intelligent selection yields smoother electromagnetic transients and inherent adaptability to nonlinearities, culminating in a marked reduction of torque ripple, a quasi-constant switching frequency, and enhanced low-speed stability, all without incurring significant computational overhead [34].

3.2. Fuzzy inference mechanism, rule base design, and NPC voltage vector decision process

The main idea of the proposed FDTC-NPC scheme is a FIS that replaces the traditional hysteresis comparators and switching table. This smart layer continuously maps the stator-flux error $\Delta\Phi_s$, the torque error $\Delta\Gamma_e$, and stator flux sector θ_s into the best NPC voltage vector. This improves torque smoothness, reduces ripple, and keeps a nearly constant switching frequency [35], [36]. The inputs are fuzzified using two levels for flux (Negative, Positive), five for torque (NL, NS, Z, PS, PL), and twelve 30° sectors for the flux angle, as shown in Figure 9. A rule-based approach, created from the drive's dynamic behavior, determines the best voltage vector to reduce errors and keep neutral-point balance. Each fuzzy rule follows the form:

$$R_i = \text{if } (\Delta\Phi_s = A_j) \text{ and } (\Delta\Gamma_e = B_k) \text{ and } (\theta_s = S_l) \text{ then } (V_{\alpha\beta} = V_m) \tag{19}$$

Where A_j, B_k and S_l represent fuzzy sets for flux, torque, and sector, and V_m denotes one of the 27 possible inverter vectors.

$$V_{\alpha\beta} = \frac{\int_\Omega \mu(V) V dV}{\int_\Omega \mu(V) dV} \tag{20}$$

This enables seamless transitions between vectors and prevents oscillations of torque. The entire rule base can be viewed as a whole from Table 3, it maps each of the twelve regions $N_1 - N_{12}$ to individual control actions. The logic for these selections considers high voltage vectors for torque correction as its top choice, followed by medium and finally small voltage vectors for fine-tuned control [37], [38].

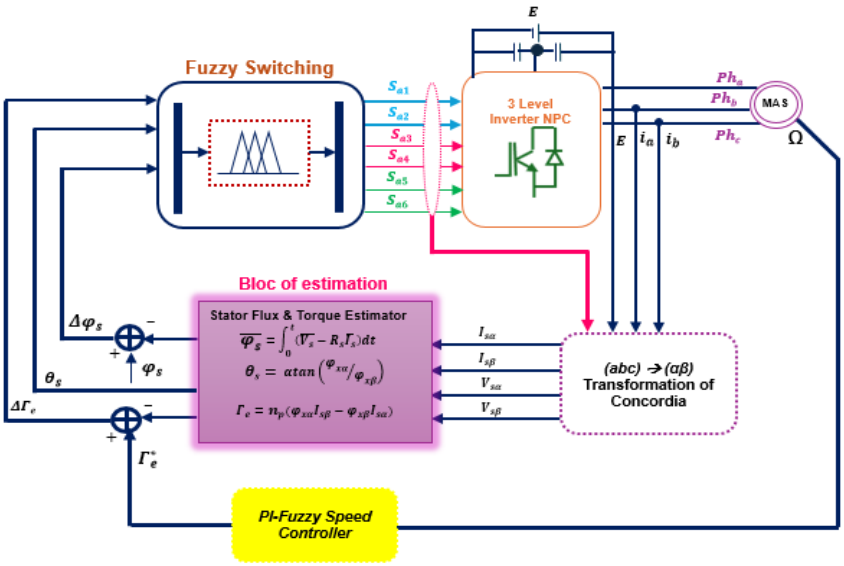

Figure 8. Structure of the proposed FDTC scheme for a three-level NPC inverter-fed IM

In the FDTC scheme, output membership functions are assigned directly to the inverter's voltage vectors. This method allows for flexible decision-making and removes the sudden state changes common in hysteresis comparators. The outcome is a smoother torque response, less flux oscillation, and better steady-state performance in three-level NPC inverter-fed drives [16], [21], [25].

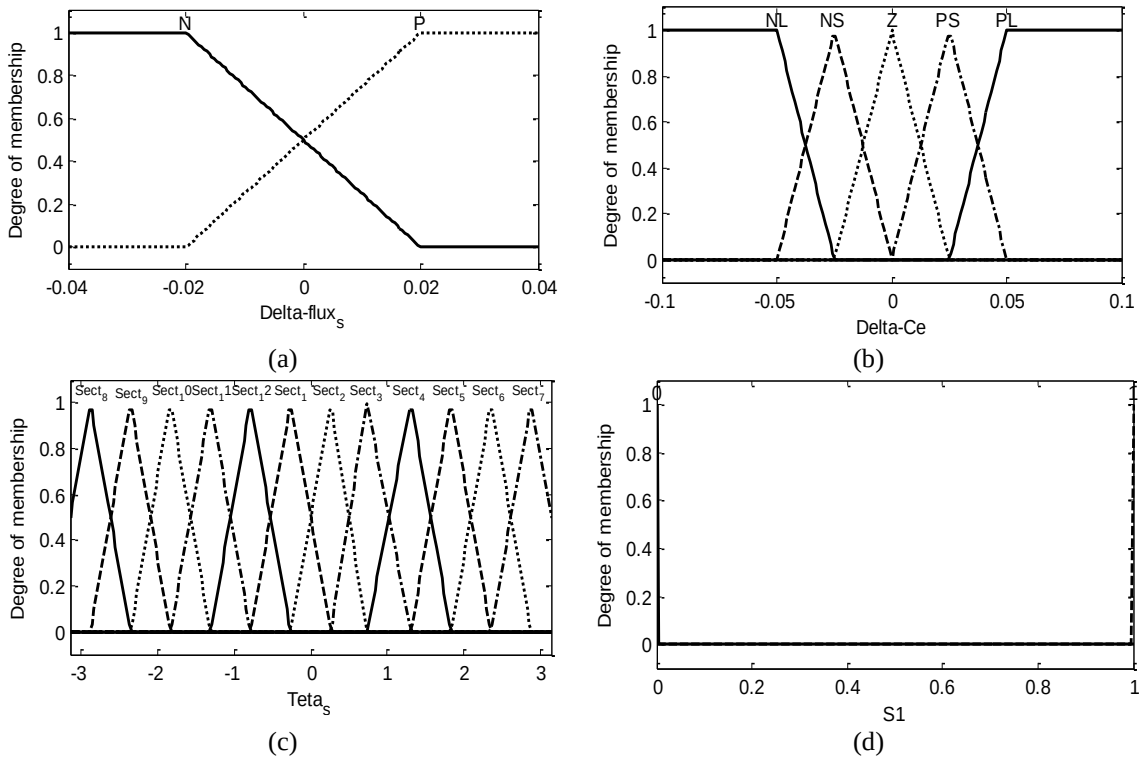

Figure 9. Membership functions of the fuzzy controller input and output variables: (a) membership functions of stator-flux error, (b) membership functions of torque error, (c) membership functions for stator-flux angle, and (d) membership functions of the output control variable

Table 3. Rule-based switching table for FDTC (Each 30° sector defines the voltage-vector selection based on flux and torque fuzzy states)

N_1			N_2			N_7			N_8		
C_{Te}/C_r	1	0	C_{Te}/C_r	1	0	C_{Te}/C_r	1	0	C_{Te}/C_r	1	0
Pl	V_5	V_8	Pl	V_5	V_8	Pl	V_{14}	V_{17}	Pl	V_{14}	V_{17}
PS	V_4	V_7	PS	V_4	V_7	PS	V_{13}	V_{16}	PS	V_{13}	V_{16}
Z	V_{19}	V_{20}	Z	V_{20}	V_{19}	Z	V_{19}	V_{20}	Z	V_{20}	V_{19}
NS	V_{16}	V_{13}	NS	V_{16}	V_{13}	NS	V_7	V_4	NS	V_7	V_4
NL	V_{17}	V_{14}	NL	V_2	V_{17}	NL	V_8	V_5	NL	V_{11}	V_5
N_3			N_4			N_9			N_{10}		
C_{Te}/C_r	1	0	C_{Te}/C_r	1	0	C_{Te}/C_r	1	0	C_{Te}/C_r	1	0
Pl	V_8	V_{11}	Pl	V_8	V_{11}	Pl	V_{17}	V_2	Pl	V_{17}	V_2
PS	V_7	V_{10}	PS	V_7	V_{10}	PS	V_{16}	V_1	PS	V_{16}	V_1
Z	V_{19}	V_{20}	Z	V_{20}	V_{19}	Z	V_{19}	V_{20}	Z	V_{20}	V_{19}
NS	V_1	V_{16}	NS	V_1	V_{16}	NS	V_{10}	V_7	NS	V_{10}	V_7
NL	V_2	V_{17}	NL	V_5	V_2	NL	V_{11}	V_8	NL	V_{14}	V_{11}
N_5			N_6			N_{11}			N_{12}		
C_{Te}/C_r	1	0	C_{Te}/C_r	1	0	C_{Te}/C_r	1	0	C_{Te}/C_r	1	0
Pl	V_{11}	V_{14}	Pl	V_{11}	V_{14}	Pl	V_2	V_5	Pl	V_2	V_5
PS	V_{10}	V_{13}	PS	V_{10}	V_{13}	PS	V_1	V_4	PS	V_1	V_4
Z	V_{19}	V_{20}	Z	V_{20}	V_{19}	Z	V_{19}	V_{20}	Z	V_{20}	V_{19}
NS	V_4	V_1	NS	V_4	V_1	NS	V_{13}	V_{10}	NS	V_{13}	V_{10}
NL	V_5	V_2	NL	V_8	V_5	NL	V_{14}	V_{11}	NL	V_{17}	V_{14}

3.3. PI-fuzzy speed controller synthesis

The FDTC-NPC machine's performance is controlled by its external speed loop. In order to improve the flexibility and overcome the fixed-gain constraint of a traditional IP controller, the paper also introduces a control strategy using a hybrid control approach called the "PI-fuzzy regulator". It combines the proportional-integral control strategy for accurate control in a short span of time with the 'fuzzy' action of the fuzzy inference system [39], [40]. Figure 10 shows the process of controlling the speeds using the error in speeds, i.e., the actual speed, $e = \Omega^* - \Omega*$, the actual speed's derivative $^{de}/_{dt}$, of the speeds. The result's influence on the proportional integral gains is utilized, which acts on the actual speed reference, ensuring an optimal torque [41].

The fuzzification process defines seven linguistic terms for each input variable (NB, NM, NS, Z, PS, PM, PB). Fuzzification uses triangular membership functions with seven linguistic terms for all variables: NB: negative big, NM: negative medium, NS: negative small, PB: positive big, PS: positive small, PM: positive medium, and ZR: zero.

Table 4 lists the fuzzy rules that relate the error and its rate of change to control actions, while Figure 11 shows the corresponding membership functions. This rule-based fuzzy structure provides smooth control dynamics with inherent nonlinearity adaptation. By dynamically modulating the control effort, it minimizes overshoot, improves settling time, and enhances disturbance rejection. The resulting PI–fuzzy controller thereby ensures robust adaptive speed regulation across the entire operating range, forming a synergistic integration with the FDTC–NPC scheme [42].

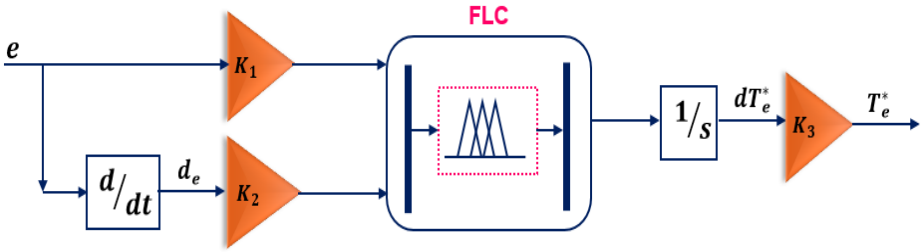

Figure 10. Block diagram of the PI-fuzzy speed controller

Table 4. Fuzzy rules for the PI-fuzzy speed controller
(Each rule defines the output control action according to the error and its derivative)

$^{d_e}/_e$	PB	PM	PS	ZR	NS	NM	NB
NB	EZ	NS	NM	NB	NB	NB	NB
NM	PS	EZ	NS	NM	NB	NB	NB
NS	PM	PS	EZ	NS	NM	NB	NB
ZR	PB	PM	PS	EZ	NS	NM	NB
PS	PB	PB	PM	PS	EZ	NS	NM
PM	PB	PB	PB	PM	PS	EZ	NS
PB	PB	PB	PB	PB	PM	PS	EZ

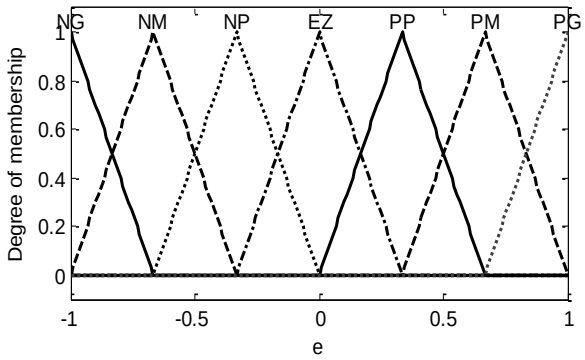

Figure 11. Membership functions of the PI fuzzy controller inputs and output

4. SIMULATION RESULTS AND DISCUSSION

4.1. Simulation setup and modeling

The proposed FDTC–NPC system was implemented in MATLAB/Simulink R2022b by integrating the flux and torque estimation blocks, the fuzzy voltage-vector selection mechanism, and the hybrid PI–fuzzy speed regulator introduced in section 3. The total simulation layout is depicted in Figure 12, and Figure 13 illustrates the detailed structure of the fuzzy DTC controller and its coupling with the three-level NPC inverter. The proposed layout provides a practical simulation environment for evaluating the performance of the drive system.

The parameters involved in the simulation process of the electrical, mechanical, and inverter systems are provided in Table 5. The design of the experiment has been conducted in a way that it is able to evaluate the transient response as well as the steady-state response of the induction motor drive system under various loading and speeds. The design of the experiment allows one to make a comparison between the traditional DTC method and the proposed FDTC/NPC method.

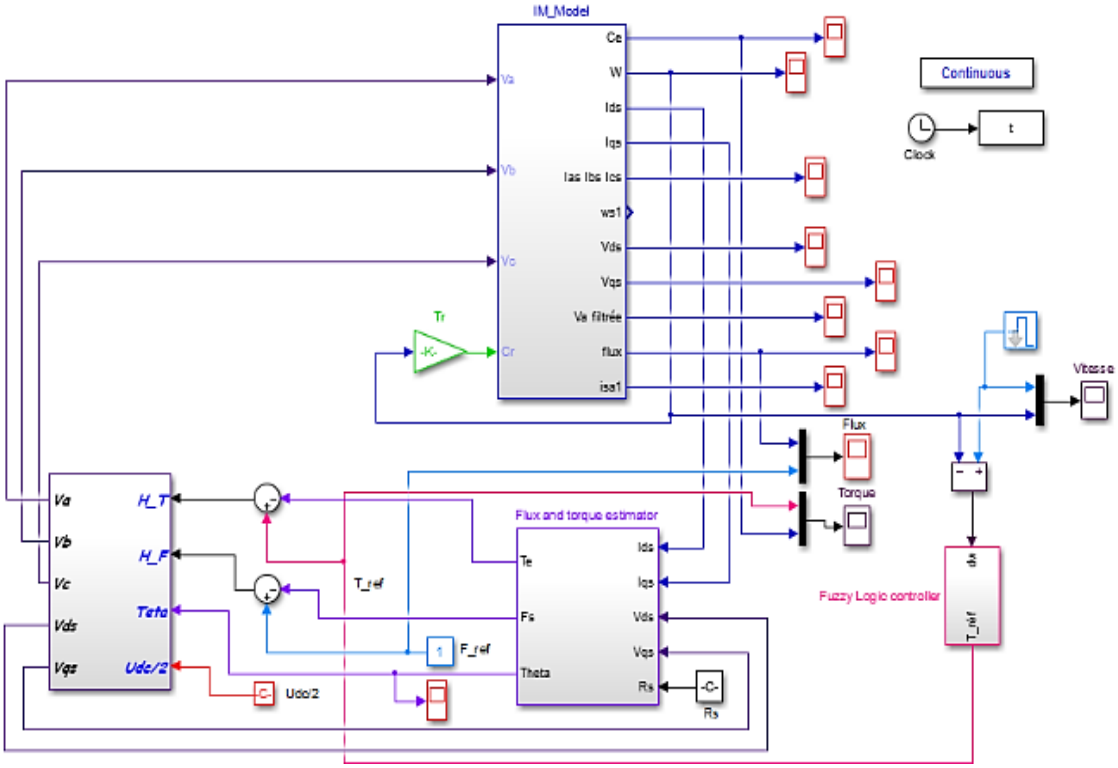

Figure 12. MATLAB/Simulink model of the proposed FDTC–NPC induction motor drive

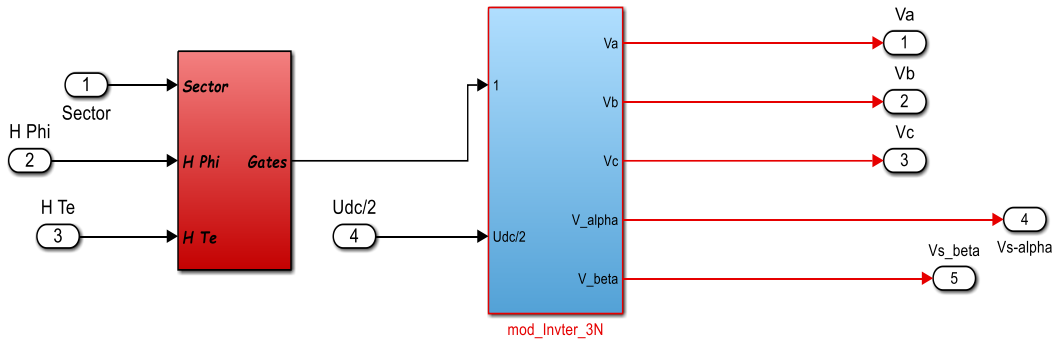

Figure 13. Internal structure of the proposed FDTC scheme

4.2. Test conditions and speed response

Simulations were carried out on a 1.5 kW induction motor over 4 s, with reference speed steps applied a t= 0.2 s (600 rpm), $t = 1.4\,s$ (1000 rpm), and $t = 3\,s$ (200 rpm). Both the IP and PI-fuzzy controllers were tested under identical conditions for fair comparison. Figure 14 illustrates that although both control methods are tracking well, the PI Fuzzy controller has far better dynamics, since it has quicker convergence, zero overshoot, and smoother transitions. The zoomed graph emphasizes its improved damping and stability when subjected to loading during acceleration and deceleration.

Table 5. IM and inverter parameters used in the simulation

Parameter	Symbol	Value	Unit
Rated power	P	1.5	kW
Voltage	V	220/380	V
Number of pair poles	n_p	2	-
Stator resistance	R_s	5.63	Ω
Rotor resistance	R_r	2.62	Ω
Stator self-inductance	L_s	0.018	H
Rotor self-inductance	L_r	0.018	H
Mutual inductance	M	0.20	H
Rotor inertia	J	0.02	kgm^2
Viscous friction coefficient	f	0.0057	$N.m.s$

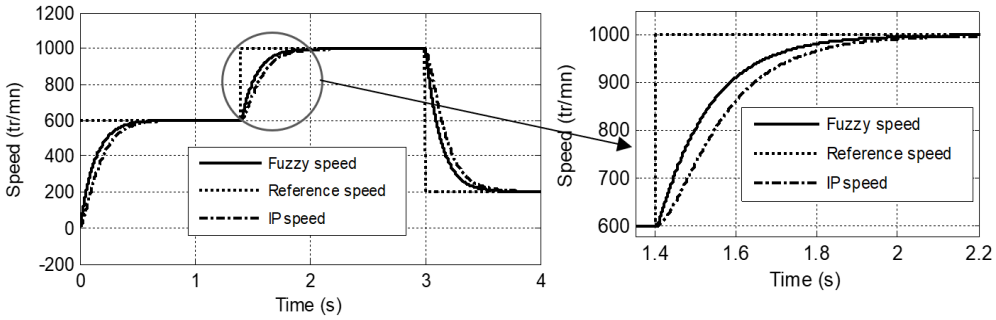

Figure 14. Rotor speed response comparison between IP controller and PI-fuzzy controller

4.3. Stator flux response

It follows that Figure 15 compares the stator flux trajectories, which show an almost perfectly circular trajectory with constant amplitude for the proposed FDTC–NPC and the distorted trajectory of conventional DTC. This improvement is due to the NPC's finer voltage resolution and fuzzy decision layer, both of which contribute to easier transitions of flux and less ripple [43].

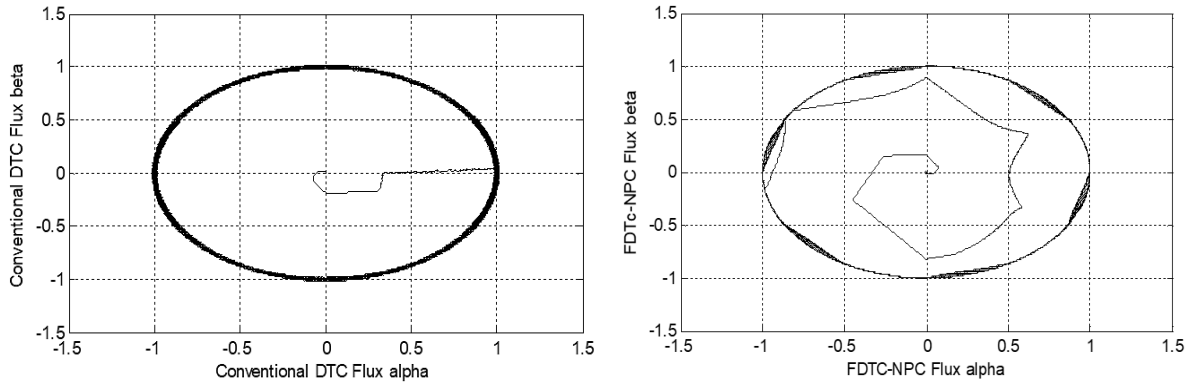

(a) (b)

Figure 15. Stator flux response: (a) conventional DTC and (b) proposed FDTC-NPC strategy

4.4. Stator current response

Figure 16 illustrates the stator current waveforms using conventional DTC and the FDTC-NPC approach. This results in smoother and sinusoidal current waveforms, unlike those produced using conventional DTC, which contain higher distortion and oscillations. This indicates that conventional DTC has poorer current control. This improvement is attributed to the three-level inverter's smaller voltage steps and fuzzy-based vector selection, which reduce current harmonics and switching stress.

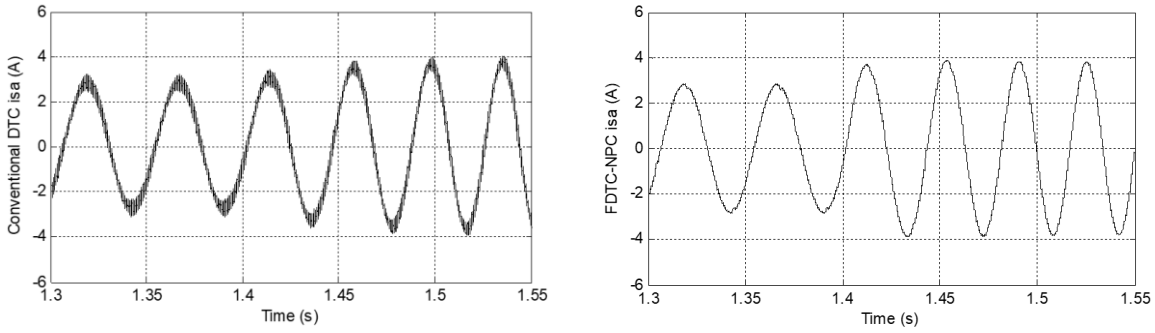

(a) (b)

Figure 16. Stator current response i_{sa}: (a) conventional DTC and (b) proposed FDTC-NPC strategy

4.5. Electromagnetic torque response

Figure 17 shows a comparison between the electromagnetic torque responses of the conventional DTC and the proposed FDTC–NPC control. The classical DTC presents strong torque ripples and irregular oscillations, while the FDTC–NPC achieves smoother and more stable responses with faster dynamic recovery. Torque ripple is lowered by nearly 25–30% due to fuzzy voltage-vector selection and the extended switching states of the three-level NPC inverter [44]. For clear comparison, the quantitative analysis confirms that torque smoothness is significantly improved by the proposed FDTC–NPC strategy, while current THD is reduced and the settling time is shortened compared with classical DTC [45], [46].

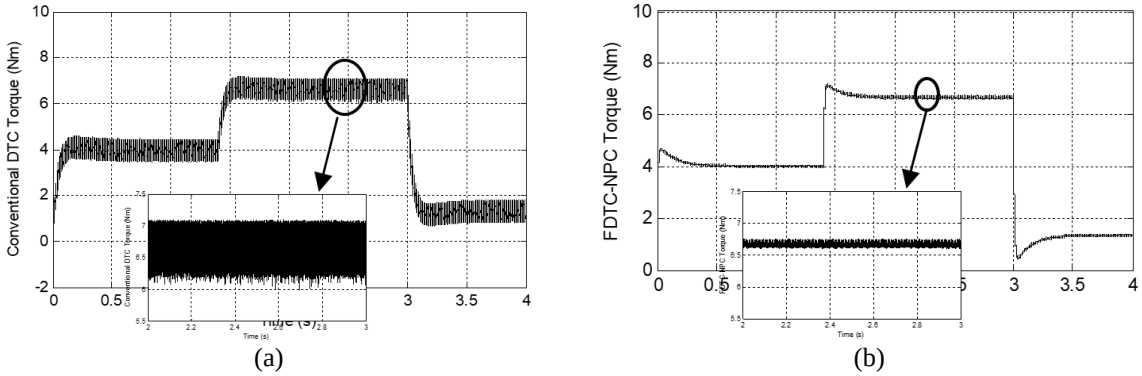

(a) (b)

Figure 17. Comparison of electromagnetic torque response and torque ripple:
(a) conventional DTC strategy and (b) proposed FDTC–NPC strategy

5. CONCLUSION

This paper introduced the FDTC strategy in IM drives based on a three-level NPC inverter. The strategy replaces the hysteresis comparators and the switching tables of the traditional DTC strategy with a fuzzy inference system. It also incorporates a speed regulator based on a PI-Fuzzy controller. Simulation outcomes have confirmed that the FDTC strategy based on the NPC inverter provides a smoother torque, an improved flux, a reduced torque ripple of around 25-30%, a lower current distortion, and improved speed tracking performance compared to the traditional DTC strategy.

FUNDING INFORMATION

The authors state that no funding was received to support this study.

AUTHOR CONTRIBUTIONS STATEMENT

This journal uses the Contributor Roles Taxonomy (CRediT) to recognize individual author contributions, reduce authorship disputes, and facilitate collaboration.

Name of Author	C	M	So	Va	Fo	I	R	D	O	E	Vi	Su	P	Fu
Jamila Chennane	✓	✓	✓	✓	✓	✓	✓	✓	✓	✓				
Lahcen Ouboubker	✓	✓	✓	✓	✓	✓				✓	✓	✓		
Mohamed Akhsassi	✓	✓	✓	✓	✓	✓				✓	✓	✓		

C : **C**onceptualization
M : **M**ethodology
So : **So**ftware
Va : **Va**lidation
Fo : **Fo**rmal analysis
I : **I**nvestigation
R : **R**esources
D : **D**ata Curation
O : Writing - **O**riginal Draft
E : Writing - Review & **E**diting
Vi : **Vi**sualization
Su : **Su**pervision
P : **P**roject administration
Fu : **Fu**nding acquisition

CONFLICT OF INTEREST STATEMENT

The authors declare no conflict of interest.

DATA AVAILABILITY

The data that are required to verify the results obtained in this article are available from the corresponding author on a reasonable request. The simulation models and numerical data obtained are made in "MATLAB/Simulink." These models can also be shared for research use.

REFERENCES

[1] J. Chennane, L. Ouboubker, N. Ettalabi, J. Lamterkati, and M. Akhsassi, "IP-self-tuning fuzzy logic controller based on direct torque control to improve induction machine speed control," in *Lecture Notes in Networks and Systems*, vol. 1098 LNNS, 2024, pp. 448–460, doi: 10.1007/978-3-031-68650-4_43.

[2] L. Ouboubker, J. Lamterkati, M. Khafallah, and A. El Afia, "Real time implementation of anti-windup PI controller for speed control of induction machine based on DTC strategy," *International Journal of Power Electronics and Drive Systems (IJPEDS)*, vol. 12, no. 3, pp. 1358–1368, Sep. 2021, doi: 10.11591/ijpeds.v12.i3.pp1358-1368.

[3] O. Lahcen, K. Mohamed, L. Jawad, E. A. Aziz, and C. Hamid, "Dspace based experimental results of direct torque control (DTC) of induction machine with speed control using IP controller," *Journal of Engineering and Applied Sciences*, vol. 13, no. 9, pp. 2672–2679, 2018, doi: 10.3923/jeasci.2018.2672.2679.

[4] I. Takahashi and T. Noguchi, "A new quick-response and high-efficiency control strategy of an induction motor," *IEEE Transactions on Industry Applications*, vol. IA-22, no. 5, pp. 820–827, Sep. 1986, doi: 10.1109/TIA.1986.4504799.

[5] M. Depenbrock, "Direct self-control (DSC) of inverter-fed induction machine," *IEEE Transactions on Power Electronics*, vol. 3, no. 4, pp. 420–429, Oct. 1988, doi: 10.1109/63.17963.

[6] L. Romeral, A. Arias, E. Aldabas, and M. G. Jayne, "Novel direct torque control (DTC) scheme with fuzzy adaptive torque-ripple reduction," *IEEE Transactions on Industrial Electronics*, vol. 50, no. 3, pp. 487–492, Jun. 2003, doi: 10.1109/TIE.2003.812352.

[7] D. Jinlian and T. Li, "Improvement of direct torque control low-speed performance by using fuzzy logic technique," in *2006 International Conference on Mechatronics and Automation*, IEEE, Jun. 2006, pp. 2481–2485, doi: 10.1109/ICMA.2006.257741.

[8] Z. Ibrahim and E. Levi, "A comparative analysis of fuzzy logic and PI speed control in high-performance AC drives using experimental approach," *IEEE Transactions on Industry Applications*, vol. 38, no. 5, pp. 1210–1218, Sep. 2002, doi: 10.1109/TIA.2002.802993.

[9] Y.-S. Lai and J.-C. Lin, "New hybrid fuzzy controller for direct torque control induction motor drives," *IEEE Transactions on Power Electronics*, vol. 18, no. 5, pp. 1211–1219, Sep. 2003, doi: 10.1109/TPEL.2003.816193.

[10] P. Cortes, M. P. Kazmierkowski, R. M. Kennel, D. E. Quevedo, and J. Rodriguez, "Predictive control in power electronics and drives," *IEEE Transactions on Industrial Electronics*, vol. 55, no. 12, pp. 4312–4324, Dec. 2008, doi: 10.1109/TIE.2008.2007480.

[11] S. M. Gadoue, D. Giaouris, and J. W. Finch, "Artificial intelligence-based speed control of DTC induction motor drives—a comparative study," *Electric Power Systems Research*, vol. 79, no. 1, pp. 210–219, Jan. 2009, doi: 10.1016/j.epsr.2008.05.024.

[12] J. Rodriguez, J.-S. Lai, and F. Z. Peng, "Multilevel inverters: a survey of topologies, controls, and applications," *IEEE Transactions on Industrial Electronics*, vol. 49, no. 4, pp. 724–738, Aug. 2002, doi: 10.1109/TIE.2002.801052.

[13] J. Rodriguez, S. Bernet, B. Wu, J. O. Pontt, and S. Kouro, "Multilevel voltage-source-converter topologies for industrial medium-voltage drives," *IEEE Transactions on Industrial Electronics*, vol. 54, no. 6, pp. 2930–2945, Dec. 2007, doi: 10.1109/TIE.2007.907044.

[14] L. Ouboubker, M. Khafallah, J. Lamterkati, and K. Chikh, "Comparison between DTC using a two-level inverters and DTC using a three level inverters of induction motor," in *2014 International Conference on Multimedia Computing and Systems (ICMCS)*, IEEE, Apr. 2014, pp. 1051–1058, doi: 10.1109/ICMCS.2014.6911167.
[15] C. C. Lee, "Fuzzy logic in control systems: fuzzy logic controller. I," *IEEE Transactions on Systems, Man, and Cybernetics*, vol. 20, no. 2, pp. 404–418, 1990, doi: 10.1109/21.52551.
[16] C. C. Lee, "Fuzzy logic in control systems: fuzzy logic controller. II," *IEEE Transactions on Systems, Man, and Cybernetics*, vol. 20, no. 2, pp. 419–435, 1990, doi: 10.1109/21.52552.
[17] M. S. Zaky, H. A. Maksoud, and H. Z. Azazi, "Sensorless induction motor drives using adaptive flux observer at low frequencies," *Engineering, Technology & Applied Science Research*, vol. 8, no. 1, pp. 2572–2576, Feb. 2018, doi: 10.48084/etasr.1752.
[18] H. Abu-Rub, J. Holtz, J. Rodriguez, and Ge Baoming, "Medium-voltage multilevel converters—state of the art, challenges, and requirements in industrial applications," *IEEE Transactions on Industrial Electronics*, vol. 57, no. 8, pp. 2581–2596, Aug. 2010, doi: 10.1109/TIE.2010.2043039.
[19] S. Kouro *et al.*, "Recent advances and industrial applications of multilevel converters," *IEEE Transactions on Industrial Electronics*, vol. 57, no. 8, pp. 2553–2580, Aug. 2010, doi: 10.1109/TIE.2010.2049719.
[20] A. Benevieri, S. Cosso, A. Formentini, M. Marchesoni, M. Passalacqua, and L. Vaccaro, "Advances and perspectives in multilevel converters: a comprehensive review," *Electronics*, vol. 13, no. 23, p. 4736, Nov. 2024, doi: 10.3390/electronics13234736.
[21] Y. Zhang and H. Yang, "Model predictive torque control of induction motor drives with optimal duty cycle control," *IEEE Transactions on Power Electronics*, vol. 29, no. 12, pp. 6593–6603, Dec. 2014, doi: 10.1109/TPEL.2014.2302838.
[22] F. Korkmaz, İ. Topaloglu, and H. Mamur, "Fuzzy logic based direct torque control of induction motor with space vector modulation," *International Journal on Soft Computing, Artificial Intelligence and Applications*, vol. 2, no. 6, pp. 33–42, Dec. 2013, doi: 10.5121/ijscai.2013.2603.
[23] M. N. Uddin, T. S. Radwan, and M. A. Rahman, "Performances of fuzzy-logic-based indirect vector control for induction motor drive," *IEEE Transactions on Industry Applications*, vol. 38, no. 5, pp. 1219–1225, Sep. 2002, doi: 10.1109/TIA.2002.802990.
[24] M. A. Perez, S. Bernet, J. Rodriguez, S. Kouro, and R. Lizana, "Circuit topologies, modeling, control schemes, and applications of modular multilevel converters," *IEEE Transactions on Power Electronics*, vol. 30, no. 1, pp. 4–17, Jan. 2015, doi: 10.1109/TPEL.2014.2310127.
[25] P. W. Hammond, "A new approach to enhance power quality for medium voltage AC drives," *IEEE Transactions on Industry Applications*, vol. 33, no. 1, pp. 202–208, 1997, doi: 10.1109/28.567113.
[26] P. F. Seixas, M. A. Severo Mendes, P. Donoso-Garcia, and A. M. N. Lima, "A space vector PWM method for three-level voltage source inverters," in *APEC 2000. Fifteenth Annual IEEE Applied Power Electronics Conference and Exposition (Cat. No.00CH37058)*, 2000, vol. 1, pp. 549–555. doi: 10.1109/APEC.2000.826157.
[27] S. Kouro, B. Wu, A. Moya, E. Villanueva, P. Correa, and J. Rodriguez, "Control of a cascaded H-bridge multilevel converter for grid connection of photovoltaic systems," in *2009 35th Annual Conference of IEEE Industrial Electronics*, Nov. 2009, pp. 3976–3982. doi: 10.1109/IECON.2009.5415332.
[28] M. N. Uddin and M. Hafeez, "FLC based DTC scheme to improve the dynamic performance of an IM drive," in *2010 IEEE Industry Applications Society Annual Meeting*, IEEE, Oct. 2010, pp. 1–7, doi: 10.1109/IAS.2010.5614089.
[29] R. Khanna, M. Singla, and G. Kaur, "Fuzzy logic based direct torque control of induction motor," in *2009 IEEE Power & Energy Society General Meeting*, IEEE, Jul. 2009, pp. 1–5, doi: 10.1109/PES.2009.5275957.
[30] G.-M. Sung, L.-F. Tung, C.-C. Huang, and H.-Y. Huang, "Modified predictive direct torque control ASIC with multistage hysteresis and fuzzy controller for a three-phase induction motor drive," *Electronics*, vol. 11, no. 11, p. 1802, Jun. 2022, doi: 10.3390/electronics11111802.
[31] A. Moussaoui, D. Ben Attous, H. Benbouhenni, Y. Bekakra, B. Nedjadi, and Z. M. S. Elbarbary, "Enhanced direct torque control based on intelligent approach for doubly-fed induction machine fed by three-level inverter," *Heliyon*, vol. 10, no. 21, p. e39738, Nov. 2024, doi: 10.1016/j.heliyon.2024.e39738.
[32] F. Berrabah, A. Chebabhi, S. Zeghlache, and S. Saad, "Direct torque control of induction motorfed by three-level inverter using fuzzy logic," *Advances in Modelling and Analysis C*, vol. 72, no. 4, pp. 248–265, Dec. 2017, doi: 10.18280/ama_c.720404.
[33] X. del Toro, S. Calls, M. G. Jayne, P. A. Witting, A. Arias, and J. L. Romeral, "Direct torque control of an induction motor using a three-level inverter and fuzzy logic," in *2004 IEEE International Symposium on Industrial Electronics*, 2004, pp. 923–927 vol. 2. doi: 10.1109/ISIE.2004.1571937.
[34] D. Casadei, G. Serra, and K. Tani, "Implementation of a direct control algorithm for induction motors based on discrete space vector modulation," *IEEE Transactions on Power Electronics*, vol. 15, no. 4, pp. 769–777, Jul. 2000, doi: 10.1109/63.849048.
[35] W. Song, S. Le, X. Wu, and Y. Ruan, "An improved model predictive direct torque control for induction machine drives," *Journal of Power Electronics*, vol. 17, no. 3, pp. 674–685, May 2017, doi: 10.6113/JPE.2017.17.3.674.
[36] S. Mencou, M. Ben Yakhelf, and E. Tazi, "Enhancing DTC control of IM using fuzzy logic and three-level inverter: a comparative study," *Turkish Journal of Electrical Engineering and Computer Sciences*, vol. 32, no. 5, pp. 732–745, Sep. 2024, doi: 10.55730/1300-0632.4098.
[37] G. Gatto, I. Marongiu, A. Serpi, and A. Perfetto, "A predictive direct torque control of induction machines," in *2008 International Symposium on Power Electronics, Electrical Drives, Automation and Motion*, Jun. 2008, pp. 1103–1108. doi: 10.1109/SPEEDHAM.2008.4581129.
[38] P. Cortes, J. Rodriguez, C. Silva, and A. Flores, "Delay compensation in model predictive current control of a three-phase inverter," *IEEE Transactions on Industrial Electronics*, vol. 59, no. 2, pp. 1323–1325, Feb. 2012, doi: 10.1109/TIE.2011.2157284.
[39] W. Xu, W. Li, W. Jiang, S. Li, and W. Wang, "Research on typical decay-like fracture defects of composite insulators based on electro-thermal coupling," *Electronics*, vol. 13, no. 22, p. 4495, Nov. 2024, doi: 10.3390/electronics13224495.
[40] C. Zhu, Y. Wang, and L. Hou, "Improved direct torque control for induction motor with fuzzy-PI controllers," in *Proceedings of the International Conference on Logistics, Engineering, Management and Computer Science*, 2015, doi: 10.2991/lemcs-15.2015.144.
[41] G. Dyanamina and S. K. Kakodia, "Adaptive neuro fuzzy inference system based decoupled control for neutral point clamped multi level inverter fed induction motor drive," *Chinese Journal of Electrical Engineering*, vol. 7, no. 2, pp. 70–82, Jun. 2021, doi: 10.23919/CJEE.2021.000017.

[42] M. Oussama, H. Lallouani, and B. Saad, "Direct torque control with space vector modulation using interval type 2 fuzzy logic regulators of dual star induction machine fed by two three-level neutral point clamped inverter," *Revue Roumaine des Sciences Techniques Serie Electrotechnique et Energetique*, vol. 69, no. 2, pp. 159–164, Jul. 2024, doi: 10.59277/RRST-EE.2024.2.7.
[43] R. Chacko and S. S. Beevi, "Improved DTC using three-level inverter topology for wind power applications," in *2013 Annual IEEE India Conference (INDICON)*, IEEE, Dec. 2013, pp. 1–5, doi: 10.1109/INDCON.2013.6726076.
[44] K.-B. Lee, J.-H. Song, I. Choy, and J.-Y. Yoo, "Torque ripple reduction in DTC of induction motor driven by three-level inverter with low switching frequency," *IEEE Transactions on Power Electronics*, vol. 17, no. 2, pp. 255–264, Mar. 2002, doi: 10.1109/63.988836.
[45] L. Tang, L. Zhong, M. F. Rahman, and Y. Hu, "A novel direct torque controlled interior permanent magnet synchronous machine drive with low ripple in flux and torque and fixed switching frequency," *IEEE Transactions on Power Electronics*, vol. 19, no. 2, pp. 346–354, Mar. 2004, doi: 10.1109/TPEL.2003.823170.
[46] Changliang Xia, Tao Liu, Tingna Shi, and Zhanfeng Song, "A simplified finite-control-set model-predictive control for power converters," *IEEE Transactions on Industrial Informatics*, vol. 10, no. 2, pp. 991–1002, May 2014, doi: 10.1109/TII.2013.2284558.

BIOGRAPHIES OF AUTHORS

Jamila Chennane received her engineering diploma in energy and her master's degree in electrical engineering from the Université de Technologie de Belfort-Montbéliard (UTBM), France. With over ten years of professional experience in both industrial and educational sectors, she has held key roles in project management, power electronics, V&V, and innovation leadership. Her expertise includes power converter design, embedded systems, battery management, and pedagogical engineering. She has contributed to projects in the aerospace and automotive industries, including collaborations with major companies. She can be contacted at email: jamila.chennane.37@edu.uiz.ac.ma.

Lahcen Ouboubker received his M.Sc. degree in Electrical Engineering from the Faculty of Sciences Semlalia, Cadi Ayyad University, Marrakech, in 2007, and his Ph.D. degree in Electrical Engineering from Hassan II University (ENSEM), Casablanca, in 2017. He obtained his HDR in 2022 from the National School of Applied Sciences, Ibn Zohr University, Agadir. He is currently an Associate Professor at the Faculty of Applied Sciences of Ait Melloul (FSAAM), Ibn Zohr University, Morocco. His research interests include advanced control of AC machines, renewable energy integration, and intelligent control of power electronic converters. He has published several papers in peer-reviewed journals and international conferences. He can be contacted at email: l.ouboubker@uiz.ac.ma.

Mohamed Akhsassi is a professor of physics at the Faculty of Applied Sciences, Ait Melloul, Ibn Zohr University, Agadir, Morocco. He earned his doctorate in energy engineering in 2019 from Cadi Ayyad University, Marrakech. His research and teaching activities focus on thermodynamics, metrology, energy storage, and renewable energy systems. He has contributed to several studies on solar energy materials, photovoltaics, and thermal analysis, with an emphasis on energy efficiency and sustainable energy management. He has published in international journals and conferences in applied physics and renewable energy. He can be contacted at email: m.akhsassi@uiz.ac.ma.